Performance Analysis for Downlink Transmission in Multiconnectivity Cellular V2X Networks

Luofang Jiao, *Member, IEEE*, Jiwei Zhao, *Member, IEEE*, Yunting Xu, *Member, IEEE*, Tianqi Zhang, *Member, IEEE*, Haibo Zhou, *Senior Member, IEEE*, and Dongmei Zhao, *Senior Member, IEEE*

***Abstract*—With the ever-increasing number of connected vehicles in the fifth-generation mobile communication networks (5G) and beyond 5G (B5G), ensuring the reliability and high-speed demand of cellular vehicle-to-everything (C-V2X) communication in scenarios where vehicles are moving at high speeds poses a significant challenge. Recently, multiconnectivity technology has become a promising network access paradigm for improving network performance and reliability for C-V2X in the 5G and B5G era. To this end, this article proposes an analytical framework for the performance of downlink in multiconnectivity C-V2X networks. Specifically, by modeling the vehicles and base stations (BSs) as 1-D Poisson point processes, we first derive and analyze the joint distance distribution of multiconnectivity. Then through leveraging the tools of stochastic geometry, the coverage probability and spectral efficiency are obtained based on the previous results for general multiconnectivity cases in C-V2X. Additionally, we evaluate the effect of the path-loss exponent and the density of downlink BS on system performance indicators. We demonstrate through extensive Monte Carlo simulations that multiconnectivity technology can effectively enhance network performance in C-V2X. Our findings have important implications for the research and application of multiconnectivity C-V2X in the 5G and B5G era.**

***Index Terms*—Cellular vehicle-to-everything (C-V2X), coverage probability, multiconnectivity, spectral efficiency, stochastic geometry.**

I. Introduction

With the evolution of the fifth-generation mobile communication networks (5G) and beyond 5G (B5G), reliable and high-performance wireless communication systems have become essential to fully exploit the potential of intelligent transportation systems (ITSs) [1], [2], [3]. Cellular vehicle-to-everything (C-V2X) has emerged as a promising technology that utilizes the existing cellular network infrastructure and spectrum to provide efficient and reliable communication between vehicles (V2V), as well as between vehicles and other network entities, such as base stations (BSs), roadside units, pedestrians, and cloud servers (V2I) [4]. This technology aims to enhance the efficiency and safety of vehicular traffic while enabling various applications such as collision avoidance, traffic management, cooperative driving, platooning, and autonomous driving, that require high-speed and low-latency communication in ITS [5], [6]. However, as the number of connected vehicles continues to increase, C-V2X is rapidly developing toward ultradense, which poses challenges such as interference management, security, and energy efficiency, and requires further research and development to enable reliable and efficient vehicular communication. C-V2X also faces significant challenges due to the high-speed mobility and dynamic topology of vehicles, which may cause rapid fluctuations in the quality of wireless links, frequent handovers, and increased signaling overhead. These challenges are severely impacting the communication performance and influence the Quality of Experience (QoE) and Quality of Service (QoS) of ITS applications.

In recent years, multiconnectivity technology has attracted significant attention to address these aforementioned challenges [7]. Multi-connectivity enables a vehicle to establish multiple simultaneous connections with different BSs using various radio access technologies (RATs), access points (APs), or channels, thus taking advantage of the diversity and availability of wireless resources in the cellular network [3]. The multiconnectivity technology, as compared to the traditional point-to-point communication, offers substantial advantages in terms of various communication performance metrics, e.g., enhanced reliability [8], improved coverage [9], and enabled seamless mobility and handover [10]. Through accessing multiple BSs, vehicles can switch between available connections without disrupting ongoing communication, providing uninterrupted connectivity even when moving across network boundaries or transiting under different coverage of networks. In addition, based on the specific requirements of the application or user preferences, multiconnectivity is capable of offering flexibility for choosing the most suitable network connections and providing better spectral efficiency by dynamic adaptation to changing network conditions [11].

Manuscript received 6 July 2023; revised 21 October 2023; accepted 5 November 2023. Date of publication 1 December 2023; date of current version 26 March 2024. This work was supported in part by the National Natural Science Foundation Original Exploration Project of China under Grant 62250004; in part by the National Natural Science Foundation of China under Grant 62271244; in part by the Natural Science Fund for Distinguished Young Scholars of Jiangsu Province under Grant BK20220067; and in part by the High-Level Innovation and Entrepreneurship Talent Introduction Program Team of Jiangsu Province under Grant JSSCTD202202. *(Corresponding author: Haibo Zhou.)*

Luofang Jiao, Jiwei Zhao, Yunting Xu, Tianqi Zhang, and Haibo Zhou are with the School of Electronic Science and Engineering, Nanjing University, Nanjing 210023, China (e-mail: luofang_jiao@smail.nju.edu.cn; jw_zhao@smail.nju.edu.cn; yuntingxu@smail.nju.edu.cn; tianqizhang@smail.nju.edu.cn; haibozhou@nju.edu.cn).

Dongmei Zhao is with the Department of Electrical and Computer Engineering, McMaster University, Hamilton, ON L8S 4L8, Canada (e-mail: dzhao@mcmaster.ca).

Digital Object Identifier 10.1109/JIOT.2023.3335233

Thus, applying multiconnectivity to C-V2X is of remarkable significance for improving communication performance and makes it more suitable for ITS applications.

In the context of multiconnectivity in C-V2X, coverage probability and spectral efficiency are two important performance metrics for evaluating wireless communication system performance [9]. However, establishing a comprehensive analytical framework with regard to these performance metrics is challenging and holds significant academic importance. following a spatial point process [12], [13]. System modeling and analytical performance evaluation based on stochastic geometry have proven to be a powerful method for monitoring the effects of important system parameters as well as optimizing system configurations, all without the need for computationally expensive and resource-intensive computer simulations [14]. Moreover, there is a research gap in the analysis of uplink and downlink performance for multiconnectivity C-V2X communication. While most of the existing studies primarily focused on the uplink transmission and performance optimization [9], [15], the downlink transmission based on an analytical framework has not been sufficiently explored. This is a significant limitation since downlink transmission plays a crucial role in supporting various ITS applications that rely on receiving downlink information from infrastructures. Therefore, conducting in-depth studies on the downlink performance of multiconnectivity C-V2X communication is substantial for filling this existing gap and ensuring a holistic analysis of the system's capabilities for supporting diverse ITS applications.

Therefore, this article considers multiconnectivity as an effective solution to resolve the challenges faced by C-V2X communication, aiming to enhance the communication performance for ITS applications. A feasible analytical framework for downlink transmission in multiconnectivity C-V2X networks is proposed by modeling the vehicles and downlink BSs (DBSs) as 1-D Poisson point processes (PPPs), the tools of stochastic geometry are used to derive crucial performance indicators, including joint distance distribution, coverage probability, and spectral efficiency. The key contributions of this article are summarized as follows.

1) We present a novel multiconnectivity performance analytical framework for C-V2X, which enables the evaluation of network performance in the 5G/B5G era. This framework provides a foundation for further research and potential performance improvement of multiconnectivity technology in C-V2X systems.
2) We derive precise expressions of coverage probability and spectral efficiency for general multiconnectivity cases in C-V2X based on the joint distance distribution. We also provide important insights into the design and optimization of C-V2X networks by analyzing the effect of path-loss exponent and DBS density on system performance indicators.
3) We conduct comprehensive Monte Carlo simulations to confirm the effectiveness of the presented multiconnectivity performance analytical framework, which shows that multiconnectivity technology can significantly improve network performance in C-V2X. This finding has important implications for the practical applications of multiconnectivity C-V2X in the 5G/B5G era.

The subsequent sections of this article are structured as follows. We briefly introduce the existing research works related to our work in Section II. Section III presents the proposed framework for analyzing multiconnectivity performance. Section IV conducts a performance analysis of the system, including the joint distance distribution, coverage probability, and spectral efficiency. In Section V, the simulation setup and results obtained from extensive Monte Carlo simulations are presented, providing verification of the proposed framework and evaluation of the system performance. Section VI presents the concluding remarks of this article.

II. Related Work

The adoption of C-V2X has emerged as a critical network paradigm for enabling vehicular communication with other vehicles and the infrastructure, offering diversified safety and efficiency applications for ITS [16]. However, despite its significant potential, the implementation of C-V2X communication is confronted with numerous challenges, such as high mobility, dynamic topology, heterogeneous network, and stringent QoS requirements [12]. In high-speed C-V2X scenarios, single connectivity with just one BS frequently leads to handover issues [7], [9], resulting in a rapid decline in communication speed and reliability, thus no longer meeting C-V2X's QoS requirements. In recent years, multiconnectivity has been considered to be a promising technology to tackle these challenges in C-V2X through enhancing reliability, reducing latency, and boosting overall network performance.

With multiple BSs access, multiconnectivity supports seamless mobility and handover between different BS coverage. Exploiting simultaneous connections, multiconnectivity offers considerable availability for the improvement of spectral efficiency [17]. A number of studies have investigated the potential benefits of applying multiconnectivity in C-V2X and wireless networks. Numerous studies have delved into the potential advantages of implementing multiconnectivity within C-V2X and wireless networks. These investigations cover various aspects, ranging from resource optimization in C-V2X multiconnectivity to performance analyses in wireless networks.

In the context of C-V2X, some studies concentrate on optimizing communication resources. Rabitsch et al. [8] explored multiconnectivity algorithms tailored to meet the stringent requirements for communication availability and latency in V2I networks. Lu et al. [7] introduced a novel approach to reduce duplication rates in DBSs in fully decoupled C-V2X networks. They achieved this by formulating and solving optimization problems using Lyapunov stochastic optimization techniques to help vehicles select access BSs for multiconnectivity and optimize bandwidth resources to meet user communication requirements. Kousaridas et al. [18] analyzed multiconnectivity management in a Manhattan model for V2X communication.

Other studies aim to evaluate the performance of multiconnectivity in both wireless networks and C-V2X scenarios. Moltchanov et al. [19] provided a closed-form upper bound on the probability density function (PDF) for multiconnectivity, shedding light on its statistical characteristics. Weedage et al. [3] scrutinized the downlink performance of multiconnectivity in wireless networks. Wu et al. [9] proposed a multiconnectivity scheme for uplink C-V2X communications, deriving precise expressions for the outage probability using stochastic geometry tools.

Numerous performance metrics have been employed in research works that explore the application of multiconnectivity technology in cellular communication scenarios. In 5G and B5G networks, Sylla et al. [20] provided a comparable cellular communication analysis for multiconnectivity. Pupiales et al. [2] focused on the multiconnectivity architectures and protocols for 5G network and they described the different network entities and protocol layers involved in multiconnectivity, such as multiconnectivity coordinator, multiconnectivity agent, multiconnectivity manager, and packet data. Petrov et al. [21] studied the dynamic characteristics of multiconnectivity technology, whereas Giordani et al. [22] investigated its application in 5G mmWave cellular networks.

In this article, we mainly focus on the performance indicator of coverage probability and spectral efficiency based on distance distribution. Coverage probability and spectral efficiency are two of the most important metrics that hold significance for evaluating the wireless networks. First, coverage probability determines the reliability of C-V2X communication in different geographical areas and network densities [13]. By leveraging multiconnectivity technology, the coverage probability can be improved and the risk of communication interruptions can be reduced. With multiple connections simultaneously receiving and transmitting data, even if one connection encounters interruption issues, the others can maintain communication, thereby enhancing overall coverage probability. Second, spectral efficiency is extremely crucial for the transmission capacity of C-V2X. C-V2X communication involves handling a substantial amount of traffic-related information, including vehicle sensor data and traffic management instructions [23]. Additional spectrum resources can be utilized in parallel or through multiplexing, thus improving spectral efficiency to support higher data transmission rates and faster response times through multiconnectivity [24]. Further improvements in coverage probability and spectral efficiency can be achieved by optimizing load balancing and resource allocation among the connections. Research in this area is of paramount importance to achieve efficient and reliable C-V2X communication, providing a more robust and efficient foundation for critical applications such as real-time vehicle communication, traffic management, and vehicular safety in ITS.

To obtain the exact analytical expression of performance metrics for multiconnectivity in C-V2X, leveraging the tools of stochastic geometry is regarded as an efficient approach and it has been increasingly popular in recent years for the performance analysis in multiconnectivity scenarios. For instance, Moltchanov et al. [19] were among the pioneers in deriving the PDF for multiconnectivity, laying essential groundwork for further investigations. Building upon this foundation, Kibria et al. [25] assessed the viability of employing dual connectivity and coordinated multiple points (CoMPs) transmission in wireless communication systems, expanding the scope of multiconnectivity applications.

Moreover, the utilization of stochastic geometry in various multiconnectivity scenarios has witnessed extensive exploration. Shafie et al. [24] explored multiconnectivity in indoor communication systems using ultrawideband terahertz (THz) technology, focusing on average ergodic capacity and connectivity likelihood. Chen et al. [12] employed coordinated multipoint techniques to enhance spectral efficiency, while Giordani et al. [22] and Kamble et al. [26] aimed to optimize the signal-to-interference-plus-noise ratio (SINR) and outage probability in single-frequency networks (SFNs). Weedage et al. [3] delved into the analysis of channel capacity and outage probability in wireless networks' downlink scenarios.

III. System Model

When analyzing the overall performance of a multiconnectivity C-V2X network, a specific vehicle is considered as a typical analysis object. Therefore, the multiple roads model can still be simplified and analyzed as a single-road situation. Moreover, it has been proven that the single road model can effectively reflect the performance of multiconnectivity in C-V2X [7], [9]. Therefore, to investigate the downlink multiconnectivity in the C-V2X scenario, we introduce a simplified 1-D system model in this article. A coordination scheme called SFNs as in [27] are leveraged for spectrum allocation. SFN enables the transmission of incoherent joint signals on the same radio resources in frequency and time, which requires BSs to coordinate when creating signals and to strictly synchronize their timing. Our focus in this article is on the intrafrequency multiconnectivity, which requires simultaneous transmission of multiple DBSs operating at the same carrier frequency to the same vehicle. This is an important issue to address in the C-V2X scenario, where high data rates and reliable communication are needed for safety-critical applications. The following of this section introduces the channel model, association policy, interference model, and performance metrics utilized in this study. Table I lists the key symbols used throughout this article.

A. Modeling of C-V2X Network

Fig. 1 shows the downlink multiconnectivity scenario in C-V2X networks. The vehicles are randomly distributed on an urban freeway segment, and the DBSs are densely distributed along the road. To simplify the analysis, we make the assumption that both the DBSs and vehicles utilize a single antenna, and denote the height difference between the antenna of the DBS and the vehicle as h.

For the tractability of the downlink performance analysis, we consider a 1-D scenario on a road including vehicles, DBSs, and interference DBSs as shown in Fig. 1, as in [6] and [9]. From a statistical perspective, the spatial distributions of vehicles and DBSs conform to 1-D PPP distributions [13], and we use the 1-D PPPs φ_V, φ_D with density λ_v, λ_d to denote the locations

TABLE I
LIST OF MAJOR SYMBOLS

Notation	Description
λ; x_i	The density of the vehicles and DBSs on a 1-D road; The distance of ith nearest DBS to the typical vehicle.
P_d; α_d	The transmit power of DBS; The downlink path loss exponent parameter.
g_d; χ_d	The channel gain between the DBS and vehicle; The Nakagami-m fading gain.
τ_D ; μ	The spectral efficiency of downlink; The mean of exponential function.
ω_d; δ_d^2	The mean of the logarithm of χ_d; The variance of the logarithm of χ_d.
φ_V, φ_D	The Poisson point processes of vehicles and DBSs.
φ_D^t; t	The DBSs set after being executed random displacement; The predetermined threshold t of coverage probability.
φ_c; Θ_I^d	The collaborative DBS set of multi-connectivity; The interference DBS set of multi-connectivity.
I_d; σ_d^2	The received interference of the typical vehicle; The noise of channel.
$\mathbb{E}(\cdot)$	The expectation of a random variable.
$\mathbb{P}(\cdot)$	The probability of a random variable.
$F(\cdot)$	The cumulative distribution function of a random variable.
$f(\cdot)$	The probability density function of a random variable.
$\zeta_I(\cdot)$	The Laplace transform of interference I.
$\Gamma(\cdot)$	The gamma distribution function of a random variable.

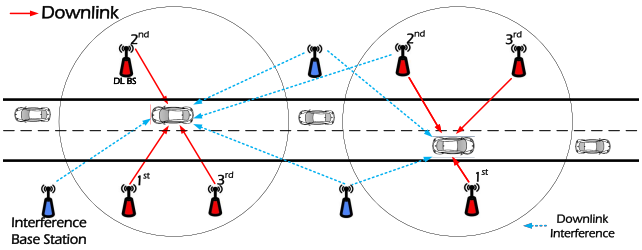

Fig. 1. Example of a practical 1-D scenario for downlink transmission in multiconnectivity C-V2X is illustrated. In this scenario, the target vehicle receives messages from the three closest DBSs, while transmissions from DBSs located beyond the collaboration distance can lead to interference to the target vehicle.

of vehicles and DBSs on the road, respectively, where φ_V, φ_D can be expressed as

$$\varphi_j \triangleq \left\{ x_{i,j} \in R^2 : i \in \mathbb{N}_+ \right\}, j = \{V, D\}.$$

All of the vehicles and DBSs are distributed along a road with length l. As per Slivnyak's theorem, the distribution of point processes remains unchanged even after adding a node at the origin [28], and in order not to lose generality and eliminate segmentation due to boundary effects, we place the typical vehicle at the origin $v_o = (0, 0)$, i.e., which represents the center of the road [9].

In relation to the formation of virtual cells, we assume that each vehicle is connected to the n nearest DBSs on a Euclidean plane. The 1-D distance between the typical vehicle v_o with the ith ($i \leq n$) DBS is r_i, thus the actual distance x_i between the transmit antenna of DBS to receive antenna of the typical vehicle is

$$x_i = \sqrt{r_i^2 + h^2}. \tag{1}$$

We adopt a common power-law path loss and Rayleigh fading model with a decay rate of $x^{-\alpha_d}$, where x denotes the distance between the DBS and the typical vehicle. The downlink path-loss exponent parameter is denoted as α_d ($\alpha_d > 2$). g_d is used to denote the power gain of Rayleigh fading and it is modeled by an exponential distribution with a mean of $1/\mu$. Therefore, we have $g_d \sim \exp(\mu)$. The distribution function of g_d is

$$f(g_d) = \mu e^{-\mu g_d}. \tag{2}$$

Furthermore, we use random variable χ_d to model the effects of shadowing between the DBS and the typical vehicle in the downlink, and χ_d follows a log-normal distribution given by $10log_{10}\chi_d \sim \aleph(\omega_d, \delta_d^2)$, where ω_d represents the mean of the logarithm of χ_d (i.e., the geometric mean of χ_d), while δ_d^2 represents the variance of the logarithm of χ_d [29]. Hence, the received signal power of the typical vehicle from the ith DBS in the downlink is [30]

$$P_{r,v}(x_i) = P_d g_d \chi_d x_i^{-\alpha_d},\ i \in \varphi_D \tag{3}$$

where P_d is the transmitting power of the DBS and is assumed to be the same for all DBSs.

B. Association Policy

The typical vehicle is assumed to be connected to n nearest DBSs by measuring all the receiving power from the nearby DBSs, finding the DBSs with the maximum receiving power (MRP) in turn [9]. Since the received power $P_{r,v}$ is not exponentially distributed for the modeling of the shadow fading [16], the lemma of random displacement theorem is considered to solve this issue [31]. Thus, $P_{r,v}(x_i) = P_d g_d \chi_d x_i^{-\alpha_d}$ can be transformed to $P_{r,v}(y_i) = P_d g_d y_i^{-\alpha_d}$, where $y_i = \chi_d^{-(1/\alpha_d)} x_i$. The 1-D PPP transformed converges to a 1-D homogeneous PPP and the intensity λ_d is transformed to $E[\chi_d^{-(1/\alpha_d)}]\lambda_d$, and the intensity of the 2-D PPP is $E[\chi_d^{-(2/\alpha_d)}]\lambda_d$ after executing the procedure of random displacement [13]. Specifically, $E[\chi_d^{-(1/\alpha_d)}]\lambda$ can be calculated as

$$\mathbb{E}\left[\chi_d^{-\frac{1}{\alpha_d}}\right]\lambda_d = \exp\left(\frac{\omega_d \ln 10}{10\alpha_d} + \frac{1}{2}\left(\frac{\sigma_d \ln 10}{10\alpha_d}\right)^2\right)\lambda_d. \tag{4}$$

Then we use 1-D PPP φ_D^t to denote the transformed set of DBS and $\lambda_D = E[\chi^{-(1/\alpha_d)}]\lambda_d$ denotes the transformed DBS intensity. To facilitate performance analysis in the following sections, we use the symbol $\varphi_D^{t,d}$ to denote the set of distances between the DBSs and the typical vehicle

$$\varphi_D^{t,d} = \{x_1, x_2, \ldots, x_i\}, i \in \mathbb{N}_+ \tag{5}$$

where x_i denotes the distance between the typical vehicle v_o and the ith nearest DBS $\in \varphi_D^t$. Thus, the candidate serving

DBSs is changed to the n nearest DBSs $\in \varphi_D^t$ in turn, and this can be expressed as

$$x_i = \underset{x_i \in \varphi_D^{t,d} \backslash \varphi_c^d}{\arg\max}\, x_i^{-\alpha_d},\ i > m \tag{6}$$

where we use $\varphi_c^d = \{x_1, x_2, \ldots, x_m\}$ to denote the set of the distances between the connected collaborative DBSs and the typical vehicle v_o at the origin, m is the number of DBSs that the typical vehicle has already connected to, and $x_i, i \in \{m+1, m+2, \ldots\}$ denotes the distance between the DBS outside φ_c^d and the typical vehicle. Let φ_c to denote the set of the connected collaborative DBSs. This means that to expand the set φ_c, we need to find the nearest DBS among DBSs in $\varphi_D^t \backslash \varphi_c$.

C. Interference

In the collaboration DBSs set φ_c, all DBSs will transmit the control and data signals simultaneously on the same subband [7]. Since the signal components of the DBSs are within the cyclic prefix, the resulting multiconnectivity SINR experienced by the typical vehicle v_o in the downlink is defined as follows:

$$\mathrm{SINR}_D = \frac{\sum_{i \in \varphi_c} P_d g_d x_i^{-\alpha_d}}{I_D + \sigma_d^2} \tag{7}$$

where $\sum_{i \in \varphi_c} P_d g_d x_i^{-\alpha_d}$ represents the sum of received signal power from the DBSs in φ_c. We use σ_d^2 to denote the power of the additive white Gaussian noise (AWGN) [14]. I_D is the power of aggregate interference from the DBSs outside of φ_c and I_D can be expressed as

$$I_D = \sum_{i \in \left\{\varphi_D^t \backslash \varphi_c\right\}} P_d g_d x_i^{-\alpha_d}. \tag{8}$$

D. Performance Metrics

In order to enable advanced C-V2X applications such as automated driving applications and stream media [4], [16], it is crucial to ensure that the downlink transmission is both reliable and capable of transmitting data at a high rate. This is important not only from the perspective of a single vehicle but also from the perspective of the whole C-V2X network. To this end, this article conducts an analytical evaluation of two performance metrics, i.e., coverage probability and spectral efficiency as follows.

1) The coverage probability of the typical vehicle v_o in the downlink is defined as the probability that the received SINR outperforms a predetermined threshold t [32]. It can be expressed as

$$\mathbb{P}_{cov}(t) = \mathbb{P}(\mathrm{SINR}_D > t). \tag{9}$$

It can also be calculated as the proportion of vehicles that have the received SINR_D above a threshold t, i.e., establish a successful connection with the DBSs in φ_c, among all vehicles in the simulation scenario. Since the cumulative distribution function (CDF) of SINR_D is $\mathbb{P}_{cov}(t) = \mathbb{P}(\mathrm{SINR}_D < t)$, the coverage probability can also be expressed as the complementary CDF (CCDF) of the SINR_D at the typical vehicle from the DBSs.

2) The spectral efficiency of the typical vehicle v_o is the amount of data transmitted per unit of bandwidth [33]. According to the Shannon theory, the spectral efficiency of the downlink is

$$\tau_D = \mathbb{E}[\ln(1 + \mathrm{SINR}_D)] \tag{10}$$

where $\mathbb{E}(\cdot)$ is the expectation function. The spectral efficiency describes the likelihood of a wireless communication system achieving a specific information amount within a certain time period and space range during actual use [23]. It can help evaluate the performance of C-V2X in a multiconnectivity environment and determine whether system optimization or adjustments are needed [33].

IV. Performance Analysis

We first derive the expression for the joint distance distribution from x_1 to x_n in this section. To optimize system configurations without the need for time-consuming computer simulations, we leverage the stochastic geometry. Specifically, by using the tools provided by stochastic geometry, we utilize the results obtained from previous sections to derive the coverage probability and spectral efficiency of C-V2X in a multiconnectivity scenario.

A. Joint Distance Distribution of the Typical Vehicle to n Service DBSs

Since the typical vehicle is connected to the n nearest DBSs in multiconnectivity, no other DBSs are closer than distance x_n. And it also means that all interference DBSs are farther than x_n. The above definition can be expressed by $f(x_1, x_2, \ldots, x_n)$, and we call it joint distance distribution for $x_1, x_2, \ldots, x_n$.

Lemma 1: The joint distance distribution of the typical vehicle to its service DBSs in set φ_c from x_1 to x_n is

$$f(x_1, x_2, \ldots, x_n) = (2\lambda_D)^n e^{-2\lambda_D x_n} \tag{11}$$

where x_n denotes the distance between the typical vehicle and the nth closest DBS in φ_c.

Proof: The null probability of a PPP in an area A is $e^{-\lambda A}$, where $A = 2\lambda x$ in 1-D PPP and $A = \pi x^2$ in 2-D PPP, thus the CCDF of x_1 is [14]

$$\begin{aligned}\mathbb{P}[x > x_1] &= \mathbb{P}[\text{no DBS closer than } x_1] \\ &= e^{-2\lambda_D x_1}.\end{aligned} \tag{12}$$

Because the $CDF = 1 - CCDF$, the CDF of x_1 is

$$F(x_1) = 1 - e^{-2\lambda_D x_1}. \tag{13}$$

Since the PDF $f(x) = [\partial F(x)/\partial x]$ [28], the PDF of x_1 is

$$f(x_1) = 2\lambda_D e^{-2\lambda_D x_1}. \tag{14}$$

According to the definition of [34, Sec. 3.3], let $f(x_2|x_1)$ denote the probability that the 2nd closest DBS is at x_2 given that the closest one is at the distance of x_1. Thus, the probability of having no DBSs between the distances x_1 and x_2 can be calculated as follows:

$$f(x_2|x_1) = 2\lambda_D e^{-2\lambda_D (x_2 - x_1)}. \tag{15}$$

According to the conditional probability Bayes theorem [35], $f(x_2, x_1)$ denotes the joint distance distribution to the two nearest distances, i.e., the probability of having at least one point in $x_2 + \Delta x$, where Δx is an infinitesimal quantity, is

$$f(x_1, x_2) = f(x_2|x_1)f(x_1) = (2\lambda_D)^2 e^{-2\lambda_D x_2}. \tag{16}$$

By following the similar procedures in (15) and (16), the joint distance distribution $f(x_1, x_2, \ldots, x_n)$ from x_1 to x_n is

$$f(x_1, x_2, \ldots, x_n) = (2\lambda_D)^n e^{-2\lambda_D x_n}. \tag{17}$$

■

To compare the joint distance distribution $f(x_1, x_2, \ldots, x_n)$ and the PDF of x_n, we provide the PDF of x_n in (18) as

$$f(x_n) = \frac{(2\lambda_b x_n)^n}{x_n \Gamma(n)} e^{-2\lambda_b x_n} \tag{18}$$

where $\Gamma(n) = (n-1)!$ when n is a positive integer.

B. Coverage Probability

A general expression for the coverage probability of multiconnectivity in C-V2X is calculated in this section.

Theorem 1: A vehicle is considered to be within the coverage area if its $SINR_D$ value from the nearest BS exceeds a certain threshold value t. On the other hand, if the $SINR_D$ falls below t, the vehicle is dropped from the network. Thus, the coverage probability of downlink for multiconnectivity C-V2X is

$$\begin{aligned}&\mathbb{P}(\mathrm{SINR}_D > t)\\ &= \int_{0<x_1<x_2<\cdots<x_m<\infty} \zeta_{I_D}(j) \exp\left(-\frac{\mu t \sigma_d^2}{\sum_{i=1}^m P_d x_i^{-\alpha_d}}\right)\\ &\times f(x_1, x_2, \ldots, x_m) dx_1 dx_2 \cdots dx_m\end{aligned} \tag{19}$$

where $j = (\mu t / [\sum_{i=1}^m P_d x_i^{-\alpha_d}])$, m is the number of cooperating DBSs in the cooperative set, $\zeta_{I_D}(j)$ is the Laplace transform of random variable interference I_D evaluated at j, and $\zeta_{I_D}(j)$ is

$$\zeta_{I_D}(j) = \exp\left[-2\lambda_D \int_{x_m}^{\infty} 1 - \frac{\mu}{jP_d x_i^{-\alpha_d} + \mu} dx_i\right]. \tag{20}$$

Proof: The proof of coverage probability in the downlink is

$$\begin{aligned}&\mathbb{P}(SINR_D > t)\\ &\overset{(a)}{=} \mathbb{P}\left(\frac{\sum_{i=1}^m P_d g_d x_i^{-\alpha_d}}{I_D + \sigma_d^2} > t\right)\\ &= \mathbb{P}\left(g_d > \frac{t(I_D + \sigma_d^2)}{\sum_{i=1}^m P_D x_i^{-\alpha_d}}\right)\\ &\overset{(b)}{=} \mathbb{E}_{x_i, I_D}\left[\exp\left(-\frac{\mu t(I_D + \sigma_d^2)}{\sum_{i=1}^m P_d x_i^{-\alpha_d}}\right)\right]\\ &\overset{(c)}{=} \mathbb{E}_{x_i}\left[\exp\left(-\frac{\mu t \sigma_d^2}{\sum_{i=1}^m P_d x_i^{-\alpha_d}}\right)\zeta_{I_D}(j)\right]\\ &= \int_{0<x_1<x_2<\cdots<x_m<\infty} \zeta_{I_D}(j) \exp\left(-\frac{\mu t \sigma_d^2}{\sum_{i=1}^m P_d x_i^{-\alpha_d}}\right)\\ &\quad \times f(x_1, x_2, \ldots, x_m) dx_1 dx_2 \cdots dx_m\end{aligned} \tag{21}$$

where (a) is obtained by substituting the expression of $SINR_D$ in (7). (b) is obtained by finding the CCDF of g_d which is exponentially distributed with parameter μ. $\zeta_{I_D}(j)$ is the Laplace transform of interference I_D in (c), and $j = (\mu t / [\sum_{i=1}^m P_d x_i^{-\alpha_d}])$. Based on the definition of the Laplace transform, the derivation of $\zeta_{I_D}(j)$ is

$$\begin{aligned}\zeta_{I_D}(j) &= \mathbb{E}_{I_D}\left[e^{-jI_D}\right]\\ &\overset{(a)}{=} \mathbb{E}_{I_D}\left[\exp\left(-j \sum_{i \in \varphi_D^t \backslash \varphi_c} P_d g_d x_i^{-\alpha_d}\right)\right]\\ &\overset{(b)}{=} \mathbb{E}_{\Theta_I^d, \{g_d\}}\left[\prod_{i \in \Theta_I^d} e^{-jP_d g_d x_i^{-\alpha_d}}\right]\\ &\overset{(c)}{=} \exp\left[-2\lambda_D \int_{x_m}^{\infty} 1\right.\\ &\quad \left. - \mathbb{E}_{g_d}\left[\exp\left(-jP_d g_d x_i^{-\alpha_d}\right)\right] dx_i\right]\\ &\overset{(d)}{=} \exp\left[-2\lambda_D \int_{x_m}^{\infty} 1 - \frac{\mu}{jP_d x_i^{-\alpha_d} + \mu} dx_i\right]\end{aligned} \tag{22}$$

where we use $\Theta_I^d = \varphi_D^t \backslash \varphi_c$ to denote the interference DBSs, interference I_D can be obtained in (8). (b) is obtained by finding the CCDF of g_d which is exponentially distributed with parameter μ. (c) is derived from the probability generating functional (PGFL) of the PPP [36], i.e.,

$$\mathbb{E}\left(\prod f(x)\right) = \exp\left(-\lambda \int_{R^2} (1 - f(x)) dx\right). \tag{23}$$

$\mathbb{E}_{g_d}[\exp(-jP_d g_d x_i^{-\alpha_d})]$ in (d) can be derived as

$$\begin{aligned}&\mathbb{E}_{g_d}\left[\exp\left(-jP_d g_d x_i^{-\alpha_d}\right)\right]\\ &= \int_0^{\infty} e^{-jP_d g_d x_i^{-\alpha_d}} \mu e^{-\mu g_d} dg_d\\ &= -\frac{\mu e^{-j\left(P_d x_i^{-\alpha_d} + \mu\right) g_d}}{jP_d x_i^{-\alpha_d} + \mu}\Big|_0^{\infty}\\ &= \frac{\mu}{jP_d x_i^{-\alpha_d} + \mu}.\end{aligned} \tag{24}$$

Since the farthest cooperation DBS is at a distance of x_m, the integration limits are from x_m to ∞ in (d). ■

C. Spectral Efficiency

This section derives the expression of spectral efficiency for the downlink by using the tools of stochastic geometry for C-V2X in multiconnectivity. We computed the spectral efficiency in units of nats/s/Hz (1 bit = ln(2) = 0.693 nats) for the typical vehicle.

Theorem 2: The spectral efficiency of the downlink in multiconnectivity C-V2X is

$$\tau_D = \int_{0<x_1<x_2<\cdots<x_m<\infty} f(x_1, x_2, \ldots, x_m) \times \mathbb{E}[\ln(1+\mathrm{SINR}_D)]dx_1dx_2\cdots dx_m \quad (25)$$

where m is the number of cooperating DBSs. $\mathbb{E}[\ln(1+\mathrm{SINR}_D)]$ is

$$\mathbb{E}[\ln(1+\mathrm{SINR}_D)] = \int_{t>0} P\left[\ln\left(1+\frac{\sum_{i=1}^{m} P_d g_d x_i^{-\alpha_d}}{I_D+\sigma_d^2}\right) > t\right]dt \quad (26)$$

where

$$\mathbb{P}\left[\ln\left(1+\frac{\sum_{i=1}^{m} P_d g_d x_i^{-\alpha_d}}{I_D+\sigma_d^2}\right) > t\right] = \exp\left(-\frac{\beta\sigma_d^2}{\sum_{i=1}^{m} P_d x_i^{-\alpha_d}}\right)\zeta_{I_D}(j) \quad (27)$$

where $\beta = \mu(e^t-1)$ and $j = (\beta/[\sum_{i=1}^{m} P_d x_i^{-\alpha_d}])$. $\zeta_{I_D}(j)$ is the Laplace transform of interference I_D, and $\zeta_{I_D}(j)$ is the same as in (22)

$$\zeta_{I_D}(j) = \exp\left[-2\lambda_D\int_{x_m}^{\infty}\left(1-\frac{\mu}{jP_d x_i^{-\alpha_d}+\mu}\right)dx_i\right]. \quad (28)$$

Proof: The proof of spectral efficiency of the downlink is

$$\begin{aligned}\tau_D &= \mathbb{E}[\ln(1+\mathrm{SINR}_D)]\\ &= \int_{0<x_1<x_2<\cdots<x_m<\infty} f(x_1, x_2, \ldots, x_m)\\ &\quad\times \mathbb{E}\left[\ln\left(1+\frac{\sum_{i=1}^{m} P_d g_d x_i^{-\alpha_d}}{I_D+\sigma_d^2}\right)\right]dx_1dx_2\cdots dx_m\\ &\overset{(a)}{=} \int_{0<x_1<x_2<\cdots<x_m<\infty} f(x_1, x_2, \ldots, x_m)\\ &\quad\times \int_{t>0}\mathbb{P}\left[\ln\left(1+\frac{\sum_{i=1}^{m} P_d g_d x_i^{-\alpha_d}}{I_D+\sigma_d^2}\right) > t\right]dtdx_1dx_2\cdots dx_m\end{aligned} \quad (29)$$

where t is the predetermined threshold. As a positive random variable X is considered, it follows that $\mathbb{E}(X)$ can be calculated as $\int_0^{\infty}\mathbb{P}(X > t)dt$ [14], thus the $\mathbb{E}[\ln(1+\mathrm{SINR}_D)]$ can be calculated in (a). Furthermore, $\mathbb{P}[\ln(1+\sum_{i=1}^{m} P_d g_d x_i^{-\alpha_d}/(I_D+\sigma_d^2)) > t]$ is

$$\begin{aligned}&\mathbb{P}\left[\ln\left(1+\frac{\sum_{i=1}^{m} P_d g_d x_i^{-\alpha_d}}{I_D+\sigma_d^2}\right) > t\right]\\ &\overset{(a)}{=}\mathbb{P}\left(\frac{\sum_{i=1}^{m} P_d g_d x_i^{-\alpha_d}}{I_D+\sigma_d^2} > e^t-1\right)\\ &\overset{(b)}{=}\mathbb{E}_{g_d}\left[g_d > \frac{(e^t-1)(I_D+\sigma_d^2)}{\sum_{i=1}^{m} P_d x_i^{-\alpha_d}}\right]\\ &\overset{(c)}{=}\mathbb{E}_{I_D}\left[\exp\left(-\frac{\mu(e^t-1)(I_D+\sigma_d^2)}{\sum_{i=1}^{m} P_d x_i^{-\alpha_d}}\right)\right]\\ &\overset{(d)}{=}\exp\left(-\frac{\beta\sigma_d^2}{\sum_{i=1}^{m} P_d x_i^{-\alpha_d}}\right)\zeta_{I_D}(j)\end{aligned} \quad (30)$$

where (a) first solves the logarithm, then calculates the expectation of the channel gain g_d in (b), and g_d follows the exponential distribution with mean $1/\mu$ in (c). Since some variables have nothing to do with I_D, they can be treated as constants and remain unchanged in (d). For the simplicity of the formula, we use $\beta = \mu(e^t-1)$ and $j = (\beta/[\sum_{i=1}^{m} P_d x_i^{-\alpha_d}])$. The Laplace transform ζ_{I_D} is the same with (22) and is omitted here. ■

D. Special Case: Single-Connectivity

In order to compare the performance with multiconnectivity in C-V2X, this section focuses on the calculation of the coverage probability and spectral efficiency in a cellular single-connectivity scenario, which represents the most basic approach. In this scenario, the typical vehicle associates with the cellular BS (CBS) with the MRP.

As the single-connectivity is a special case of multiconnectivity, we model the similar channel model as in multiconnectivity scenario, and use λ_C to denote the transformed intensity λ_c of CBS ϱ_C^t after executing the procedures of random displacement, and $\lambda_C > \lambda_D$. As the CBS are distributed along the road following a 1-D PPP, the PDF of distance distribution is

$$f(x) = 2\lambda_C e^{-2\lambda_C x} \quad (31)$$

where x is the distance between the nearest CBS and the typical vehicle.

The coverage probability of the downlink in cellular single-connectivity is

$$\mathbb{P}_{\mathrm{cov}}\left(\mathrm{SINR}_c^D > t\right) = \int_0^{\infty} 2\lambda_C e^{-\mu t\sigma_d^2 x^{\alpha_d}/P_d} e^{-2\lambda_C x}\zeta_{I_d^c}(j)dx \quad (32)$$

where $j = \mu t x^{\alpha_d}/P_d$, the SINR_c^D is

$$\mathrm{SINR}_c^D = \frac{P_d g_d x_i^{-\alpha_d}}{I_d^c+\sigma_d^2} \quad (33)$$

where the interference I_d^c is

$$I_d^c = \sum_{i\in\varrho_C^t} P_d g_d x_i^{-\alpha_d}. \quad (34)$$

The Laplace transform of I_d^c is

$$\zeta_{I_d^c}(j) = \exp\left[-2\lambda_C\int_x^{\infty} 1-\frac{\mu}{jP_d x_i^{-\alpha_d}+\mu}dx_i\right]. \quad (35)$$

Proof: Given the similarity in the proof to that of Theorem 1, we omit the specific steps here. ■

The spectral efficiency of cellular single-connectivity for downlink is

$$\tau_c^D = \int_0^{\infty} f(x)E\left[\ln\left(1+\mathrm{SINR}_c^D\right) > t\right]dx \quad (36)$$

where

$$\mathbb{E}\left[\ln\left(1+\mathrm{SINR}_c^D\right) > t\right] = \int_0^{\infty} e^{-\frac{\mu(e^t-1)x^{\alpha_d}\sigma_d^2}{P_d}}\zeta_{I_d^c}(j)dt \quad (37)$$

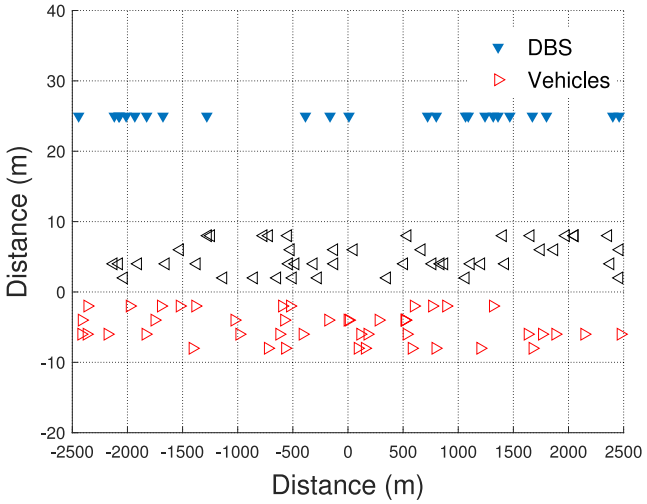

Fig. 2. Simulation scenario of multiconnectivity in C-V2X.

TABLE II
MAIN PARAMETERS

Channel Parameters	Value
DBS transmitting power P_d (dBm)	23
Pathloss exponent for downlink α_d	$2.1 \sim 6$
Noise power σ_d^2 (dBm)	-96
Mean of log-normal shadowing gain (dB)	0
Std of shadowing gain for MBS (dB)	2
Simulation parameters	**Value**
The length of road (km)	30
The number of iteration	10,000
Density of vehicle on road λ_v (nodes/km)	20
Density of DBS λ_d (nodes/km)	$0.05 \sim 5.7$
Threshold (dB)	$0 \sim 40$

where $j = \mu(e^t - 1)x^{\alpha_d}/P_d$, the $\zeta_{I_d^c}(j)$ is

$$\zeta_{I_d^c}(j) = \exp\left[-2\lambda_D \int_x^\infty \left(1 - \frac{\mu}{(e^t - 1)x^{\alpha_d} x_i^{-\alpha_d} + \mu}\right) dx_i\right] S. \tag{38}$$

Proof: The proof of spectral efficiency of downlink for cellular single-connectivity is similar to Theorem 2, the specific steps are omitted here. ■

V. Numerical and Simulation Results

A two-tier communication scenario on a straight urban freeway is considered in this section. The length of the freeway is set as 30 km. The specific simulation scenario is shown in Fig. 2. We first verify the proposed theoretical derivation in previous sections over 10 000 Monte Carlo simulations of the DBSs and vehicles following 1-D PPPs. The detailed steps of the simulation are in Simulation 1. We use "Cellu 1," "Conn 2," and "Conn 3" to abbreviate single-connectivity, dual-connectivity, and triple-connectivity, respectively, in the legends of the figures. According to [37], [38], and [39], Table II summarizes the system simulation parameters employed in this article.

A. Joint Distance Distribution

Fig. 3(a) shows the distance distribution of x_1, x_2, and x_3. We can see that the peak is gradually moving away from the origin from x_1 to x_3. Fig. 3(b) and (c) depicts the joint distance distribution for $f(x_1, x_2)$ and $f(x_1, x_2, x_3)$. We can see that the peak of $f(x_1, x_2, x_3)$ is closest to the origin, followed by $f(x_1, x_2)$, and the furthest is $f(x_1)$. Compared with distance distributions in Fig. 3(a), the peak of joint distance distribution has a huge boost. The closer the distance between the peak and the origin, the better the performance. It can be observed that in single-connectivity, $f(x_1)$ exhibits better performance. Compared to a single-connectivity, a greater number of DBSs connections in multiconnectivity lead to a more significant performance improvement.

Simulation 1: Simulation for Multi-Connectivity in C-V2X

Input: simulation number n, road length l, threshold t, DBS density λ_d, vehicle density λ_v;
Output: Coverage probability CP, spectral efficiency τ_D;

Initialize $\tau_{\mathbf{o}} \leftarrow \mathbf{0}_{n\times\lambda_v l}$, $\mathbf{P} \leftarrow \mathbf{0}_{n\times\lambda_v l}$, $CP_n \leftarrow \mathbf{0}_{1\times n}$, $\tau_n \leftarrow \mathbf{0}_{1\times n}$
for $i = 1; i \le n; i++$ **do**
  Generate the locations $\mathbf{m}$, $\mathbf{V}$ of DBSs and vehicles following 1-D PPP, respectively;
  for $v = 1; v \le \lambda_v l; v++$ **do**
    Select collaborative DBSs according to Eq. (6);
    Calculate $SINR_D$ of DL according to Eq. (7);
    $\tau_{\mathbf{o}}(i, v) = \ln(1 + SINR_D)$, $\mathbf{P}(i, v) = SINR_D$;
  end
  $CP_n(i) = \sum_{i=1}^{\lambda_v l}(\mathbf{P}(i, :) > t)/(\lambda_v l)$;
  $\tau_n(i) = \sum_{i=1}^{\lambda_v l}\tau_{\mathbf{o}}(i,:)/(\lambda_v l)$;
end
Return $\tau_D = \sum_{i=1}^{n}\tau_n(i)/n$, $CP = \sum_{i=1}^{n}CP_n(i)/n$;

B. Coverage Probability

The coverage probability variation of downlink with threshold t is illustrated in Fig. 4. It is apparent that the simulation values closely match the theoretical values, which further verifies the validity of the theoretical derivation results. The density of BS λ_c in single-connectivity is set as 3 nodes/km, and the density λ_d of DBSs in multiconnectivity is set as 6 nodes/km. Though $\lambda_c > \lambda_d$, we can see that the dual-connectivity and triple-connectivity still have a greater coverage probability than single-connectivity. This suggests that multi-connectivity performs better than cellular single-connectivity in C-V2X and multiconnectivity enhances the coverage area of communications.

Fig. 5 illustrates the coverage probability as a function of path-loss exponent α_d. It can be seen that the Monte Carlo simulation data and analytical data fit well. Considering the dense deployment of DBSs in the simulation, vehicles are in an interference-limited state. At this moment, the interference power will decrease in accordance with the increase of α_d, which in turn leads to a promotion of SINR. Therefore, the coverage probability will be improved even if the channel gain decreases.

For a better investigation of the impact of path-loss exponent α_d on the coverage probability under different densities of

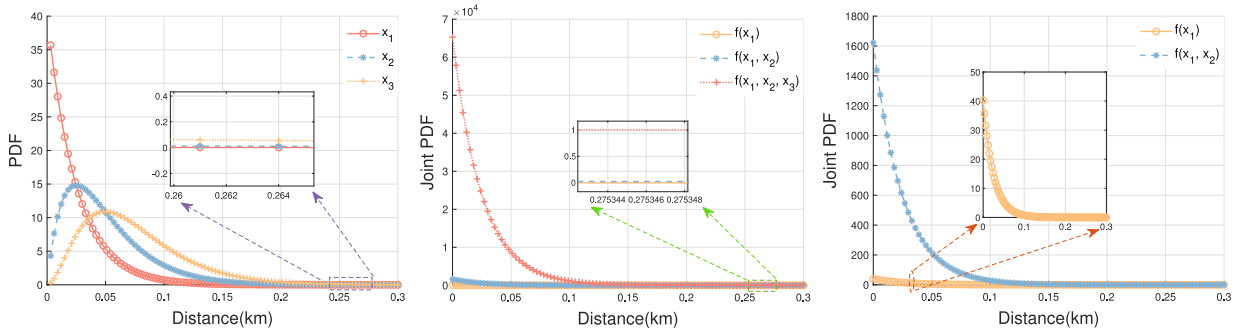

Fig. 3. Distance distributions $f(x_i)$ and joint distance distribution $f(x_1, x_2, \ldots, x_m)$ under different distances. (a) Distance distribution for nearest distances x_1, x_2, and x_3. (b) Joint distance distribution of $f(x_1), f(x_1, x_2)$, and $f(x_1, x_2, x_3)$. (c) Since $f(x_1)$ and $f(x_1, x_2)$ are much smaller than $f(x_1, x_2, x_3)$, the two functions are highlighted here.

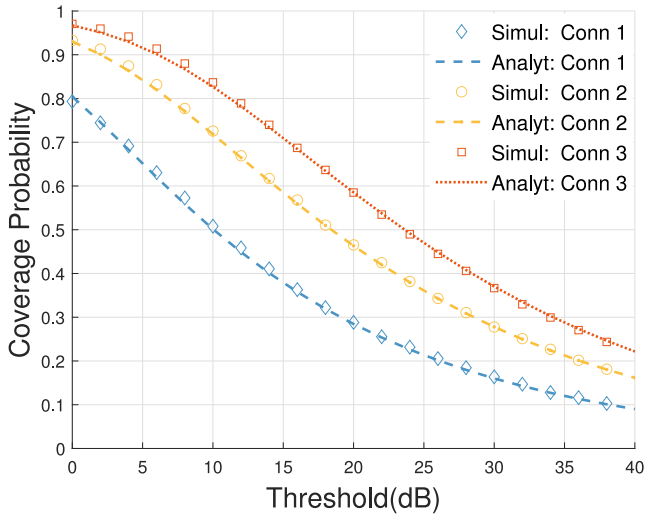

Fig. 4. Coverage probability variation with threshold t $t \in [0, 40]$ ($\lambda_d = 3$ nodes/km, $\lambda_c = 6$ nodes/km).

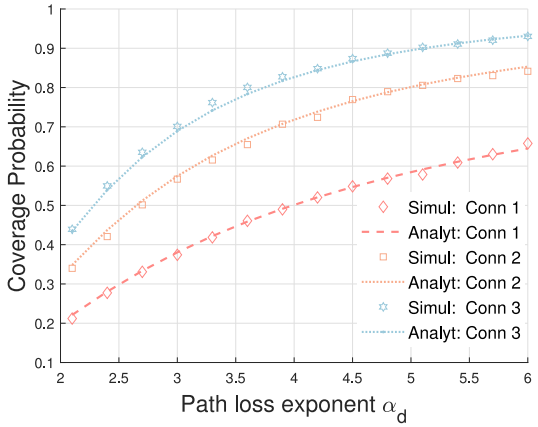

Fig. 5. Effect of path-loss exponent on coverage probability ($\alpha_d \in [2.1, 6]$).

DBSs, we plot Fig. 6 in a dual-connectivity scenario. As shown in Fig. 6, when the density of DBSs is in a dense deployment, the system is an interference-limited network. The distance between the signal DBSs $\in \varphi_c$ and the interference DBSs is close to the typical vehicle, so the increase of α_d leads to a

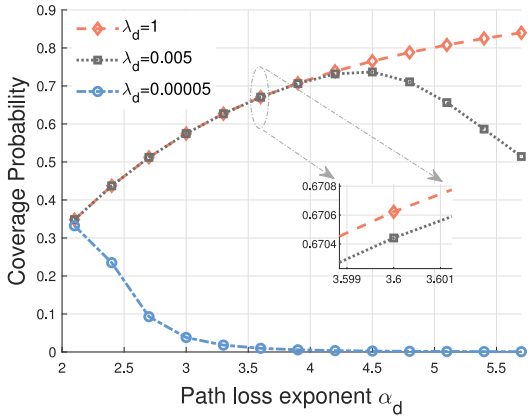

Fig. 6. Coverage probability of dual-connectivity varies with different path-loss exponent in different densities of DBSs α_d (2.1–5.7).

greater impact on the interference signal power, resulting in an increase in the coverage probability. However, when the density is low enough, the system can be considered as a noise-limited network. Both the signal DBSs and the interference DBSs are far away from the typical vehicle, so the increase of α_d has a greater impact on the receiving signal power, leading to a continuous decrease in the coverage probability. When the density λ_d is at an appropriate size, such as $\lambda_d = 0.005$ nodes/km, the coverage probability first increases and then decreases with the increase of α_d.

The coverage probability of all cases decreases as the threshold t increases, while the difference between single-connectivity and multiconnectivity first increases and then decreases in Fig. 7. This is mainly because the coverage probability is, respectively, high and low at small and large thresholds, respectively. Only when the threshold value is in the middle range, the difference in coverage probability is large, and the advantage of applying multiconnectivity is also demonstrated. It can be observed that increasing the number of connected DBSs does not result in a proportional increase in the coverage probability gain. Hence, at a particular threshold, there exists a balance tradeoff between the number of corporation DBSs that are connected and the associated cost.

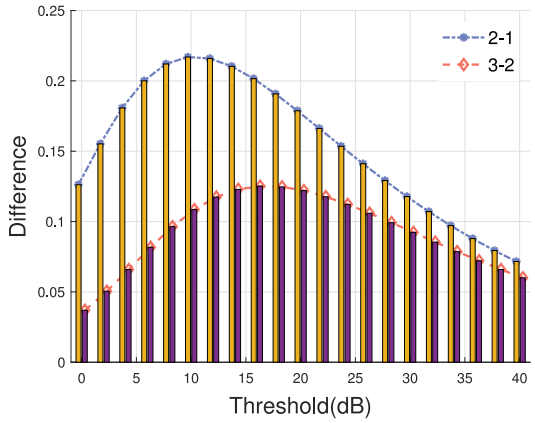

Fig. 7. Coverage probability differences variation with threshold t (0–40 dB).

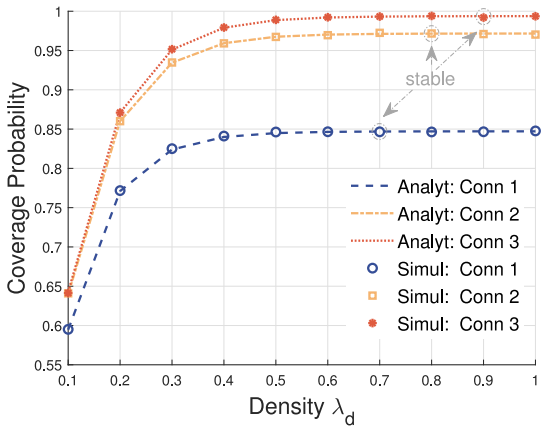

Fig. 8. Coverage probability variation with BS density λ_d (0.1–1 nodes/km).

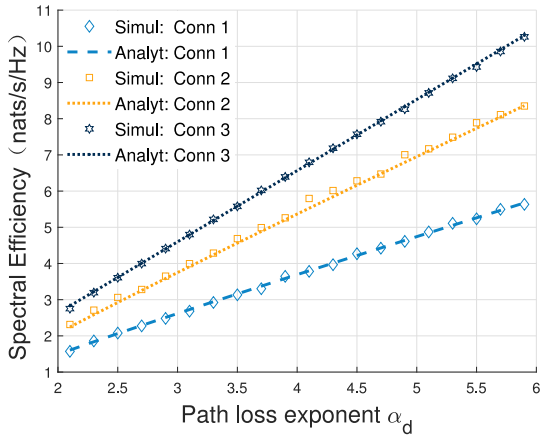

Fig. 9. Spectral efficiency variation with the path-loss exponent α_d (2.1–5.9).

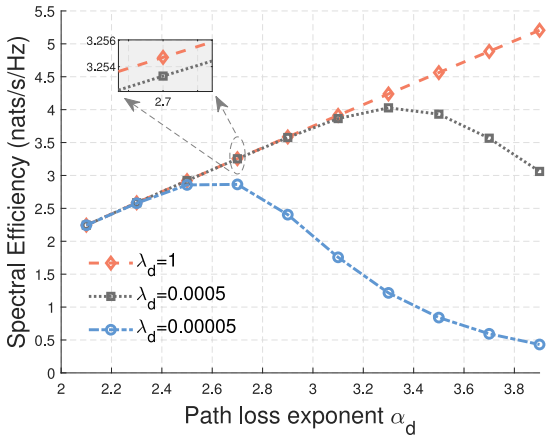

Fig. 10. Spectral efficiency of dual-connectivity varies with different path-loss exponent in different densities of DBSs α_d (2.1–3.9).

As shown in Fig. 8, the coverage probability varies with the density λ_d of DBSs. The coverage probability goes up first and then stays relatively constant for both cellular single-connectivity and multiconnectivity when the density λ_d increases. It can also be seen that the growth rate of multiconnection is faster than that of single-connection, and it also reaches a stable point later. At the same time, it can be seen that the coverage probability does not increase significantly when comparing triple-connectivity to dual-connectivity. Therefore, increasing the number of cooperative BSs can improve the communication coverage area, but it may also incur high costs. By observing the horizontal axis, it can be noted that the change in DBS density λ_d is relatively small in magnitude. This implies that the coverage probability is sensitive to changes in λ_d, and suggests that simply increasing λ_d does not necessarily lead to an improvement in coverage probability.

C. Spectral Efficiency

The spectral efficiency varies with the path-loss exponent α_d is illustrated in Fig. 9. The simulation data is represented by the points and the theoretical data is represented by the dashed line in Fig. 9. We can observe that the simulation data matches the theoretical data well, demonstrating the correctness of the theoretical derivation. The increase of path-loss exponent leads to a gradual increase in spectral efficiency and an approximately linear relationship. The reason is that, as the dense deployment of DBSs, vehicles are in an interference-limited state, with the increase of path-loss exponent α_d, the interference signals weaken more than the signals transmitted by the cooperative BSs, resulting in an increase in SINR and consequently spectral efficiency. It appears that there exists a close-to-linear relationship between the path-loss exponent α_d, mainly because after dividing the received signal power $\sum_{i\in\varphi_c} P_d g_d x_i^{-\alpha_d}$ into the denominator of (9), since the thermal noise is much smaller than the received signal and thus $\sigma_d^2 / \sum_{i\in\varphi_c} P_d g_d x_i^{-\alpha_d} \approx 0$, then after logarithmic calculation, it approximates to a linear relationship. Fig. 10 depicts the spectral efficiency of dual-connectivity as a function of α_d in different densities of DBSs. Since the spectral efficiency is mainly affected by SINR, it can be seen that the trend of spectral efficiency is similar to that of coverage probability in Fig. 6 when the DBSs layout changes from extremely dense to extremely sparse.

Fig. 11 plots the spectral efficiency improvements between the multiconnectivity and single-connectivity. It can be observed

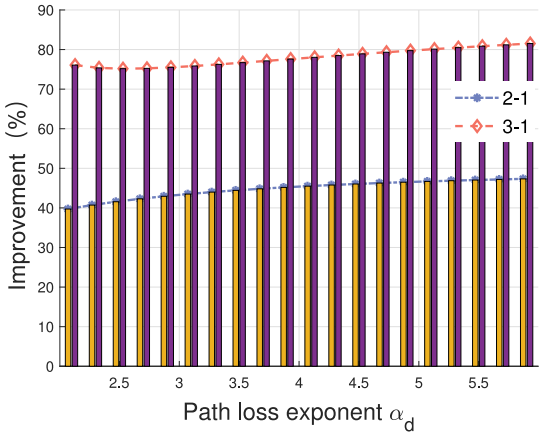

Fig. 11. Spectral efficiency percentage increase of multiconnectivity compared to single-connectivity.

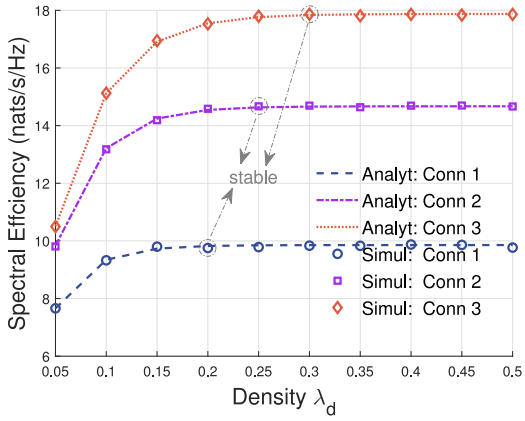

Fig. 12. Spectral efficiency as a function of BS density λ_d (0.05–0.5 nodes/km).

that the application of multiconnectivity technology greatly improves the spectral efficiency in C-V2X. The improvement achieved by dual-connectivity can reach up to 40%, and that achieved by triple-connectivity can increase to more than 75%. With the increase of path-loss exponent α_d, the performance improvement of spectral efficiency does not increase significantly. This indicates that multiconnectivity technology has a stable performance gain.

Fig. 12 illustrates the spectral efficiency varies with the DBS density λ_d. With the increase of λ_d, the spectral efficiency first improves and then remains stable. Moreover, the improvement of multiconnectivity is greater than that of single-connectivity, and the stable point is also further back. This means that multiconnectivity has a larger range of performance improvement. Similar to Fig. 8, adding too many DBSs does not continuously improve spectral efficiency. Additionally, it can be observed that the stable point of spectral efficiency arrives earlier than the stable point of coverage probability. Thus, when increasing the density of DBSs λ_d, it is necessary to comprehensively consider the demands between spectral efficiency and coverage probability.

VI. Conclusion

This article has demonstrated the potential of enhancing network performance in C-V2X by using the proposed multiconnectivity performance analysis framework. By analyzing performance indicators, such as coverage probability and spectral efficiency in the downlink, this article has provided insights into the effect of path-loss exponent and the density of DBS on the system performance indicators. The extensive Monte Carlo simulations have effectively validated the proposed framework and demonstrated the effectiveness of multiconnectivity technology in enhancing the performance of C-V2X networks. The results of this article have important implications for the research and practical applications of multiconnectivity C-V2X in the 5G and B5G era, and further investigations are warranted to explore the full potential of this technology for next-generation communication systems.

References

[1] A. Wolf, P. Schulz, M. Dörpinghaus, J. C. S. S. Filho, and G. Fettweis, "How reliable and capable is multi-connectivity?" *IEEE Trans. Commun.*, vol. 67, no. 2, pp. 1506–1520, Feb. 2019.

[2] C. Pupiales, D. Laselva, Q. De Coninck, A. Jain, and I. Demirkol, "Multi-connectivity in mobile networks: Challenges and benefits," *IEEE Commun. Mag.*, vol. 59, no. 11, pp. 116–122, Nov. 2021.

[3] L. Weedage, C. Stegehuis, and S. Bayhan, "Impact of multi-connectivity on channel capacity and outage probability in wireless networks," *IEEE Trans. Veh. Technol.*, vol. 72, no. 6, pp. 7973–7986, Jun. 2023.

[4] Y. Xu, H. Zhou, T. Ma, J. Zhao, B. Qian, and X. Shen, "Leveraging multiagent learning for automated vehicles scheduling at nonsignalized intersections," *IEEE Internet Things J.*, vol. 8, no. 14, pp. 11427–11439, Jul. 2021.

[5] S. Chen et al., "Vehicle-to-everything (V2X) services supported by LTE-based systems and 5G," *IEEE Commun. Stand. Mag.*, vol. 1, no. 2, pp. 70–76, Jul. 2017.

[6] J. Chen, G. Mao, C. Li, W. Liang, and D.-G. Zhang, "Capacity of cooperative vehicular networks with infrastructure support: Multiuser case," *IEEE Trans. Veh. Technol.*, vol. 67, no. 2, pp. 1546–1560, Feb. 2018.

[7] Z. Lu, T. Zhang, X. Ji, B. Qian, L. Jiao, and H. Zhou, "Personalized wireless resource allocation in multi-connectivity B5G C-V2X networks," in *Proc. 14th Int. Conf. Wireless Commun. Signal Process. (WCSP)*, 2022, pp. 1–6.

[8] A. Rabitsch et al., "Utilizing multi-connectivity to reduce latency and enhance availability for vehicle to infrastructure communication," *IEEE Trans. Mobile Comput.*, vol. 21, no. 5, pp. 1874–1891, May 2022.

[9] P. Wu, L. Ding, Y. Wang, L. Li, H. Zheng, and J. Zhang, "Performance analysis for uplink transmission in user-centric ultra-dense V2I networks," *IEEE Trans. Veh. Technol.*, vol. 69, no. 9, pp. 9342–9355, Sep. 2020.

[10] F. B. Tesema, A. Awada, I. Viering, M. Simsek, and G. Fettweis, "Evaluation of context-aware mobility robustness optimization and multi-connectivity in intra-frequency 5G ultra dense networks," *IEEE Wireless Commun. Lett.*, vol. 5, no. 6, pp. 608–611, Dec. 2016.

[11] L. Diez, A. G.-Saavedra, V. Valls, X. Li, X. C.-Perez, and R. Agüero, "LaSR: A supple multi-connectivity scheduler for multi-RAT OFDMA systems," *IEEE Trans. Mobile Comput.*, vol. 19, no. 3, pp. 624–639, Mar. 2020.

[12] S. Chen, T. Zhao, H.-H. Chen, Z. Lu, and W. Meng, "Performance analysis of downlink coordinated multipoint joint transmission in ultra-dense networks," *IEEE Netw.*, vol. 31, no. 5, pp. 106–114, Aug. 2017.

[13] V. V. Chetlur and H. S. Dhillon, "Coverage analysis of a vehicular network modeled as Cox process driven by Poisson line process," *IEEE Trans. Wireless Commun.*, vol. 17, no. 7, pp. 4401–4416, Jul. 2018.

[14] J. G. Andrews, F. Baccelli, and R. K. Ganti, "A tractable approach to coverage and rate in cellular networks," *IEEE Trans. Commun.*, vol. 59, no. 11, pp. 3122–3134, Nov. 2011.

[15] L. P. Qian, Y. Wu, H. Zhou, and X. Shen, "Non-orthogonal multiple access vehicular small cell networks: Architecture and solution," *IEEE Netw.*, vol. 31, no. 4, pp. 15–21, Jul./Aug. 2017.

[16] K. Yu, H. Zhou, Z. Tang, X. Shen, and F. Hou, "Deep reinforcement learning-based RAN slicing for UL/DL decoupled cellular V2X," *IEEE Trans. Wireless Commun.*, vol. 21, no. 5, pp. 3523–3535, May 2022.
[17] Y. Xu, B. Qian, K. Yu, T. Ma, L. Zhao, and H. Zhou, "Federated learning over fully-decoupled RAN architecture for two-tier computing acceleration," *IEEE J. Sel. Areas Commun.*, vol. 41, no. 3, pp. 789–801, Mar. 2023.
[18] A. Kousaridas, C. Zhou, D. Martín-Sacristán, D. Garcia-Roger, J. F. Monserrat, and S. Roger, "Multi-connectivity management for 5G V2X communication," in *Proc. IEEE 30th Annu. Int. Symp. Pers., Indoor Mobile Radio Commun. (PIMRC)*, 2019, pp. 1–7.
[19] D. Moltchanov, A. Ometov, S. Andreev, and Y. Koucheryavy, "Upper bound on capacity of 5G mmWave cellular with multi-connectivity capabilities," *Electron. Lett.*, vol. 54, no. 11, pp. 724–726, 2018.
[20] T. Sylla, L. Mendiboure, S. Maaloul, H. Aniss, M. A. Chalouf, and S. Delbruel, "Multi-connectivity for 5G networks and beyond: A survey," *Sensors*, vol. 22, no. 19, p. 7591, 2022.
[21] V. Petrov et al., "Dynamic multi-connectivity performance in ultra-dense urban mmWave deployments," *IEEE J. Sel. Areas Commun.*, vol. 35, no. 9, pp. 2038–2055, Sep. 2017.
[22] M. Giordani, M. Mezzavilla, S. Rangan, and M. Zorzi, "Multi-connectivity in 5G mmWave cellular networks," in *Proc. Mediterr. Ad Hoc Netw. Workshop (Med-Hoc-Net)*, 2016, pp. 1–7.
[23] Z. Sattar, J. V. C. Evangelista, G. Kaddoum, and N. Batani, "Spectral efficiency analysis of the decoupled access for downlink and uplink in two-tier network," *IEEE Trans. Veh. Technol.*, vol. 68, no. 5, pp. 4871–4883, May 2019.
[24] A. Shafie, N. Yang, and C. Han, "Multi-connectivity for indoor terahertz communication with self and dynamic blockage," in *Proc. IEEE Int. Conf. Commun. (ICC)*, 2020, pp. 1–7.
[25] M. G. Kibria, K. Nguyen, G. P. Villardi, W.-S. Liao, K. Ishizu, and F. Kojima, "A stochastic geometry analysis of multiconnectivity in heterogeneous wireless networks," *IEEE Trans. Veh. Technol.*, vol. 67, no. 10, pp. 9734–9746, Oct. 2018.
[26] V. Kamble, S. Kalyanasundaram, V. Ramachandran, and R. Agrawal, "Efficient resource allocation strategies for multicast/broadcast services in 3GPP long term evolution single frequency networks," in *Proc. IEEE Wireless Commun. Netw. Conf.*, 2009, pp. 1–6.
[27] M. Simsek, T. Hößler, E. Jorswieck, H. Klessig, and G. Fettweis, "Multiconnectivity in multicellular, multiuser systems: A matching-based approach," *Proc. IEEE*, vol. 107, no. 2, pp. 394–413, Feb. 2019.
[28] S. N. Chiu, D. Stoyan, W. S. Kendall, and J. Mecke, *Stochastic Geometry and Its Applications*. Hoboken, NJ, USA: Wiley, 2013.
[29] A. A. Hussein, T. A. Rahman, and C. Y. Leow, "Performance evaluation of localization accuracy for a log-normal shadow fading wireless sensor network under physical barrier attacks," *Sensors*, vol. 15, no. 12, pp. 30545–30570, 2015.
[30] V. V. Chetlur and H. S. Dhillon, "Coverage and rate analysis of downlink cellular vehicle-to-everything (C-V2X) communication," *IEEE Trans. Wireless Commun.*, vol. 19, no. 3, pp. 1738–1753, Mar. 2020.
[31] C. Xu, M. Sheng, V. S. Varma, T. Q. S. Quek, and J. Li, "Wireless service provider selection and bandwidth resource allocation in multi-tier HCNs," *IEEE Trans. Commun.*, vol. 64, no. 12, pp. 5108–5124, Dec. 2016.
[32] X. Yang and A. O. Fapojuwo, "Coverage probability analysis of heterogeneous cellular networks in Rician/Rayleigh fading environments," *IEEE Commun. Lett.*, vol. 19, no. 7, pp. 1197–1200, Jul. 2015.
[33] M. Jia, Z. Yin, Q. Guo, G. Liu, and X. Gu, "Downlink design for spectrum efficient IoT network," *IEEE Internet Things J.*, vol. 5, no. 5, pp. 3397–3404, Oct. 2018.
[34] D. Moltchanov, "Distance distributions in random networks," *Ad Hoc Netw.*, vol. 10, no. 6, pp. 1146–1166, 2012.
[35] D. Berrar, "Bayes' theorem and naive Bayes classifier," *Encycl. Bioinform. Comput. Biol. ABC Bioinform.*, vol. 403, p. 412, Sep. 2018.
[36] D. Stoyan, W. S. Kendall, S. N. Chiu, and J. Mecke, *Stochastic Geometry and its Applications*. Hoboken, NJ, USA: Wiley, 2013.
[37] "Study on evaluation methodology of new vehicle-to-everything (V2X) use cases for LTE and NR; Version 15.2.0," 3GPP, Sophia Antipolis, France, Rep. 37.885, Dec. 2018.
[38] "Coordinated multi-point operation for LTE physical layer aspects; Version 11.2.0," 3GPP, Sophia Antipolis, France, Rep. 36.819, Sep. 2013.
[39] H. Elshaer, M. N. Kulkarni, F. Boccardi, J. G. Andrews, and M. Dohler, "Downlink and uplink cell association with traditional macrocells and millimeter wave small cells," *IEEE Trans. Wireless Commun.*, vol. 15, no. 9, pp. 6244–6258, Sep. 2016.

Luofang Jiao (Member, IEEE) received the B.S. degree in detection guidance and control technology from the University of Electronic Science and Technology of China, Chengdu, China, in 2020. He is currently pursuing the Ph.D. degree with the School of Electronic Science and Engineering, Nanjing University, Nanjing, China.

His research interests include uplink/downlink-decoupled access, C-V2X, and heterogeneous networks.

Jiwei Zhao (Member, IEEE) received the M.S. degree in information and communication system from Xidian University, Xi'an, China, in 2018. He is currently pursuing the Ph.D. degree with the School of Electronic Science and Engineering, Nanjing University, Nanjing, China.

His research interests include fully decoupled RAN architecture, coordinated multipoint, and machine learning applications for wireless communication.

Mr. Zhao won the First Prize in the 2016 CCF (China Computer Federation) China Big Data and Cloud Computing Intelligence Contest.

Yunting Xu (Member, IEEE) received the B.S. degree in communication engineering from Nanjing University, Nanjing, China, in 2017, where he is currently pursuing the Ph.D. degree with the School of Electronic Science and Engineering.

He mainly focuses on the dynamic resource management and networking optimization in the field of emerging wireless networks.

Tianqi Zhang (Member, IEEE) received the B.S. degree in electronic information science and technology from Nanjing University, Nanjing, China, in 2021, where he is currently pursuing the Ph.D. degree with the School of Electronic Science and Engineering.

He mainly focuses on the FD-RAN, V2X, and machine learning in the field of emerging wireless networks.

Haibo Zhou (Senior Member, IEEE) received the Ph.D. degree in information and communication engineering from Shanghai Jiao Tong University, Shanghai, China, in 2014.

From 2014 to 2017, he was a Postdoctoral Fellow with the Broadband Communications Research Group, Department of Electrical and Computer Engineering, University of Waterloo, Waterloo, ON, Canada. He is currently a Full Professor with the School of Electronic Science and Engineering, Nanjing University, Nanjing, China. His research interests include resource management and protocol design in B5G/6G networks, vehicular ad hoc networks, and space–air–ground-integrated networks.

Prof. Zhou was a Highly Cited Researcher by Clarivate Analytics in 2022 and 2020. He was a recipient of the 2019 IEEE ComSoc Asia–Pacific Outstanding Young Researcher Award, the 2023–2024 IEEE ComSoc Distinguished Lecturer, and the 2023–2025 IEEE VTS Distinguished Lecturer. He served as the Track/Symposium Co-Chair for IEEE/CIC ICCC 2019, IEEE VTC-Fall 2020, IEEE VTC-Fall 2021, WCSP 2022, IEEE GLOBECOM 2022, and IEEE ICC 2024. He is currently an Associate Editor of the IEEE TRANSACTIONS ON WIRELESS COMMUNICATIONS, IEEE INTERNET OF THINGS JOURNAL, *IEEE Network Magazine*, and *Journal of Communications and Information Networks*. He was elected as an IET Fellow in 2022.

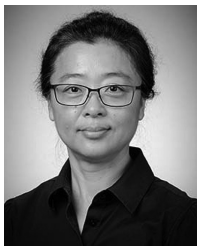

Dongmei Zhao (Senior Member, IEEE) received the B.S. degree in wireless communication from Northern Jiaotong University (currently, Beijing Jiaotong University), Beijing, China, in 1992, and the Ph.D. degree from the Department of Electrical and Computer Engineering, University of Waterloo, Waterloo, ON, Canada, in June 2002.

In July 2002, she joined the Department of Electrical and Computer Engineering, McMaster University, Hamilton, ON, Canada, where she is a Full Professor. From April 2004 to March 2009, she was an Adjunct Assistant Professor with the Department of Electrical and Computer Engineering, University of Waterloo. Her current research areas are mainly in mobile computation offloading, energy-efficient wireless networking, and vehicular communication networks.

Prof. Zhao is a Co-Chair of the Mobile and Wireless Networks Symposium of IEEE GLOBECOM Conference 2020, the Wireless Networking Symposium in IEEE GLOBECOM Conference 2007, the Green Computing, Networking, and Communications Symposium in International Conference on Computing, Networking and Communications 2020, the Technical Program Committee for IEEE International Workshop on Computer Aided Modeling and Design of Communication Links and Networks 2016, the General Symposium of the International Wireless Communications and Mobile Computing (IWCMC) Conference 2007, and the Vehicular Networks Symposium of IWCMC from 2012 to 2019. She is an Associate Editor of the IEEE INTERNET OF THINGS JOURNAL. She served as an Associate Editor for the IEEE TRANSACTIONS ON VEHICULAR TECHNOLOGY from 2007 to 2017. She also served as an Editor for *EURASIP Journal on Wireless Communications and Networking* and *Journal of Communications and Networks*. She has been on the technical program committee of many international conferences in her fields. She is a Professional Engineer of Ontario.